Broadband TM-Mode-Pass Polarization Rotator and Power Divider With Tunable Beam-Splitting Ratio

Chunyu Deng, Mengjia Lu, Yu Sun, Lei Huang, Dongyu Wang, Jingyu Zhang, Guohua Hu, Binfeng Yun, and Yiping Cui

***Abstract*—A TM-mode-pass polarization rotator and power divider with an arbitrary beam-splitting ratio constructed by an adiabatic taper, a spatial mode order convertor and a multi-mode interferometer (MMI) is proposed on the silicon-on insulator (SOI) platform. Both arbitrary power splitting and polarization selection-rotation can be realized in this single device. The measurements show that a continuously adjustable beam-splitting ratio from 1:99 to 99:1 within a 33.2 mW power consumption from 1520–1580 nm has been realized for the proposed device.**

***Index Terms*—Polarization rotator, power divider, mode conversion, integrated optics.**

I. Introduction

SILICON on insulator (SOI) is an excellent photonic integrated circuit (PIC) platform due to its strong light field limitation, low transmission loss and high divergence, compatible fabrication for complementary metal-oxide-semiconductor (CMOS) [1]. Unfortunately, large birefringence is introduced by the high refractive index contrast of the SOI platform, resulting in a strong polarization dependence of the SOI-based photonic device. On-chip polarization management device has become a key component for the SOI-based PIC, such as polarization beam splitters [2], [3], polarization beam-splitter rotators [4], polarizers [5]. Among them, the polarizer is the simplest scheme which can filter out the undesired polarized light, so as to obtain light in a single polarization state. It can be widely applied in optical communication and optical sensing systems.

In silicon photonics, an optical power divider is also a basic component, which is often utilized for power distribution or as a basic element for building more complex devices, such as modulators [6], switches [7], and multiplexers [8]. Over the years, tremendous efforts have been made and a variety of schemes have been proposed and demonstrated [9]–[12]. Notice that polarizers and power dividers are always combined together to highly enrich the choices of devices for building high-performance PICs, involving on-chip optical switching and multiplexing systems [2], [8], [13]. Designing multifunctional photonic devices that can handle both polarization states and power splitting provides additional degrees of freedom for high-density integrated photonic links. For example, by utilizing a hybrid plasmonic waveguide and a Y-splitter structure, both polarization selection and equal-power splitting can be realized in a single device [14], [15]. In addition, by using two-dimensional photonic crystals based on Bragg reflection, the integrated polarizer and power divider can be realized in a single device [16]. These solutions that integrate the polarizer and the power divider into a single device increase the space utilization of the integrated chip and expand versatile applications of the device to a certain extent. However, exploring more potential applications of the device is limited due to the fixed beam-splitting ratio. Adding another tunable degree of freedom to such a multifunctional device can further expand the application of the device.

In this paper, we propose an on-chip multi-functional device of polarization rotation and power splitting, which has the advantages of broadband and adjustable beam-splitting ratio. For the injected TM_0, with the flow of light, the transformation process of optical mode is TM_0-TE_3-TE_0, and the beam- splitting ratio is tunable. For the TE_0 mode, the proposed device behaves as an attenuator. Thus, both polarization rotator and power divider with tunable beam-splitting ratio can be realized on a single device. In addition, this device can be used as a polarizer which is because the injected TE_0 mode is blocked.

II. Structure and Design Principle

Fig. 1 shows the schematic of the proposed device, including three basic structures: an adiabatic taper, a spatial mode order convertor and a 2×2 multi-mode interferometer (MMI). The adiabatic taper is composed of a multi-segmented linear taper, which is used to rotate the polarization state of the input light. It can convert TE_0 to TE_0, or TM_0 to TE_3, which is consistent with the mode conversion in our previous work [17]. The spatial mode order convertor is composed of four S-bend waveguides and two spiral waveguides, which can realize two functions: 1) Separate TE_3 into two TE_0 with equal optical power; 2) Filter TE_0 and TM_0. The MMI is used to realize the interference between the two modulation arms, the phase difference of which can be changed by applying a voltage to the heater, and then the continuous adjustment of the beam-splitting ratio can be achieved. In order to reduce the amount of calculation, we simulate the above

Manuscript received 23 June 2022; revised 15 July 2022; accepted 28 July 2022. Date of publication 1 August 2022; date of current version 17 August 2022. This work was supported in part by the National Key Research and Development Program of China under Grant 2018YFB2201903, in part by the National Natural Science Foundation of China under Grant 62075038, and in part by National Key Research and Development Program of China under Grant 2018YFE0201000. *(Corresponding author: Guohua Hu.)*

The authors are with the Advanced Photonics Center, Southeast University, Nanjing 210096, China (e-mail: dcy@seu.edu.cn; mjlu@seu.edu.cn; 230189799@seu.edu.cn; 230189110@seu.edu.cn; 230208131@seu.edu.cn; 220201512@seu.edu.cn; photonics@seu.edu.cn; ybf@seu.edu.cn; cyp@seu.edu.cn).

Digital Object Identifier 10.1109/JPHOT.2022.3195491

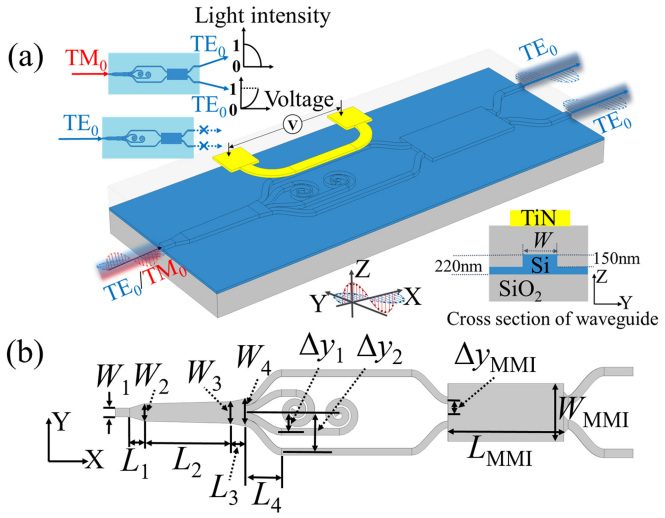

Fig. 1. (a) Schematic of the proposed polarizer and power divider on SOI waveguide. (b) Sketch of the proposed design.

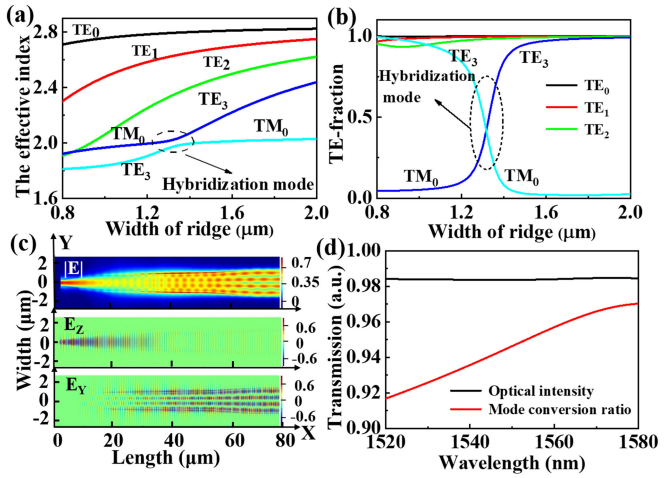

Fig. 2. (a) The calculated effective indices and (b) TE-fraction for guide modes of rib waveguide with different waveguide widths. (c) Electric fields distributions of the adiabatic taper at wavelength of 1550 nm. (d) The calculated transmittance spectra of the adiabatic taper.

three structures respectively by using 3D finite-difference time-domain method (FDTD, Ansys-Lumerical FDTD Solution).

Firstly, we analyze mode hybridization of the adiabatic taper. This adiabatic taper consists of three segment linear tapers based on rib waveguides. In this paper, the height of the rib waveguide and the slab are 220 nm and 70 nm respectively, as shown in the subgraph of Fig. 1(a). Fig. 2(a) shows the refractive indices of rib waveguides as a function of waveguide width W. It can be seen that the hybridization mode of TM_0 and TE_3 appears near $W = 1.3$ μm. To analyze the polarization states of guide modes, the TE-fraction is used to represent the ratio of the energy of TE polarization to the total energy of the mode. Specifically, the TE-fraction of each mode can be expressed as:

$$\text{TE}-\text{fraction} = \frac{\int |E_y|^2 dydz}{\int \left(|E_y|^2 + |E_z|^2\right) dydz} \quad (1)$$

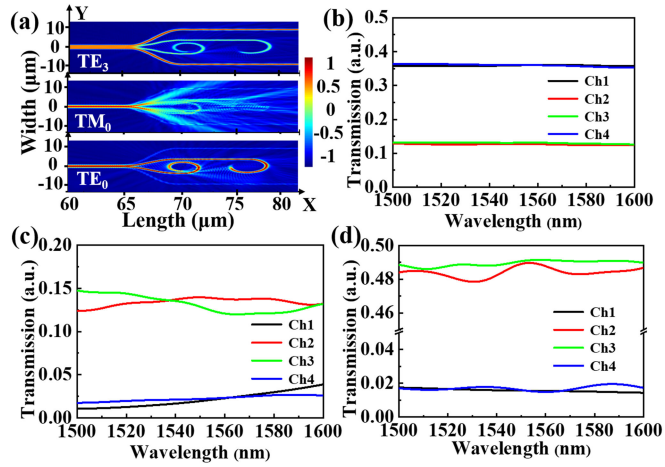

Fig. 3. (a) The optical field distribution in spatial mode order convertor at wavelength of 1550 nm. The calculated transmittance spectra of spatial mode order convertor in (b) TE_3 mode, (c) TM_0 mode and (d) TE_0 mode.

Here, E_y and E_z are the electric field components in Y and Z directions, respectively. As shown in Fig. 2(b), this hybridized mode can be seen as the combination of TE_3 and TM_0 modes. The input light can evolve from TM_0 mode to TE_3 mode by a linear taper in the hybridization mode region ($W = 1.2 \sim 1.5$ μm). The widths W_1, W_2, W_3 and W_4 of the tapered waveguides are set respectively to be 0.80 μm, 1.20 μm, 1.50 μm and 1.93 μm. The taper lengths L_1, L_2 and L_3 are 8.15 μm, 36.97 μm and 15.00 μm, respectively. The electric field distributions of the adiabatic taper are shown in Fig. 2(c). It can be seen that the major component of input light is transformed from E_z to E_y with the flow of optical energy and the input TM_0 mode is transformed to TE_3 mode. Here, the mode conversion ratio is defined as the ratio of the energy of TE_3 mode to input light energy. As shown in Fig. 2(d), the mode conversion ratio exceeds 91% in the wavelength range from 1520 nm to 1580 nm [17].

Secondly, we analyze the spatial mode order convertor. Here, the output channels of spatial mode order convertor are denoted as Ch1-Ch4 from top to bottom. The spatial mode order convertor is designed to separate the TE_3 mode into two TE_0 modes, and these signals are output from Ch1 and Ch4 respectively. At the same time, ideally, we hope that the optical energy in Ch2 and Ch3 can be coupled to the adjacent Ch1 and Ch4 as much as possible. The residual energy is consumed by the spiral waveguide or radiated into the cladding. By using a particle swarm optimization method, the optimal parameters are $\Delta y_1 = 3.00$ μm, $\Delta y_2 = 7.92$ μm and $L_4 = 10.00$ μm, respectively. In this case, the optical field distribution and transmission spectrum of spatial mode order convertor are shown in Fig. 3.

As shown in Fig. 3(a), when the TE_3 mode is input into the spatial mode order convertor, the optical energy is mainly divided into two channels and output from the upper (Ch1) and lower (Ch4) channels in TE_0 mode. The transmission spectrum of the spatial mode order convertor is shown in Fig. 3(b). It can be seen that a broad bandwidth can be achieved and at least 0.71

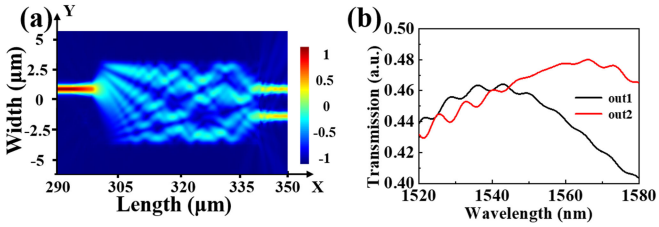

Fig. 4. (a) The optical field distribution of the proposed 2×2 MMI at wavelength of 1550 nm. (b) The calculated transmittance spectra of 2×2 MMI in TE_0 mode.

(loss< 1.49 dB) of optical energy is passed from Ch1 and Ch4 in the range of 1500–1600 nm.

In addition, the spatial mode order convertor also has the function of mode filtering. As shown in Fig. 3(a), for the input TM_0 mode, it is difficult to confine the light in S-bend waveguides, and major light energy will radiate into the cladding. In other words, if a part of the input TM_0 light is not converted to TE_3 after passing through the adiabatic taper, it will be filtered by the spatial mode order convertor. As can be seen from Fig. 3(c), the normalized light energy $(I_{Ch1}+ I_{Ch4})/I_{In}$ is lower than 0.064, which means that the PER of TM_0 mode can be filtered to 11.9 dB. Here, I_{Ch1}, I_{Ch4} and I_{In} represent the light energy of the Ch1, Ch4 and input spatial mode order convertor, respectively. The PER is defined as $-10\lg((I_{Ch1}+I_{Ch4})/I_{In})$. Similarly, for the injected TE_0 mode, the optical energy is mainly concentrated in the middle channels (Ch2 and Ch3) and then consumed by the spiral waveguide or radiated into the cladding. Specifically, as can be seen from Fig. 3(d), the PER of TE_0 mode is >14.9 dB in the wavelength range of 1500–1600 nm.

Thirdly, we analyze the 2×2 MMI. As shown in Fig. 1, the 2×2 MMI is a symmetrical structure. Here we analyze the case of light input from the upper port of the 2×2 MMI. The optimized W_{MMI}, L_{MMI} and Δy_{MMI} are 6.00 μm, 42.80 μm and 1.00 μm respectively. The optical field distribution of the proposed 2×2 MMI is shown in Fig. 4(a). It can be seen that the input light is divided into two channels after the 2×2 MMI. Within the bandwidth of 60 nm (1520–1580 nm), the insertion loss IL = $-10\lg((I_{out1}+I_{out2})/I_{in})$ of the MMI is less than 0.61 dB. Here, I_{out1}, I_{out2} and I_{in} represent the light energy of the out1 (the upper output), the out2 (the lower output) and the input port of the 2×2 MMI, respectively.

III. Experiment Results and Discussion

The proposed device can be fabricated on the regular SOI platform with a 220 nm core silicon layer and a 2 μm buried oxide layer. Firstly, the waveguide patterns can be defined by using deep ultraviolet (DUV) lithography. Then, single-step shallow etching with a height of 150 nm by inductively coupled plasma (ICP) is applied to form a rib waveguide. Next, a thin SiO_2 cladding with a height of 1 μm is deposited on the sample by plasma enhanced chemical vapor deposition (PECVD). Subsequently, transmission electrodes (Al and Cu) and thermoelectric electrodes (TiN) are fabricated respectively based on the metal lift-off technology. The optical micrograph of the fabricated

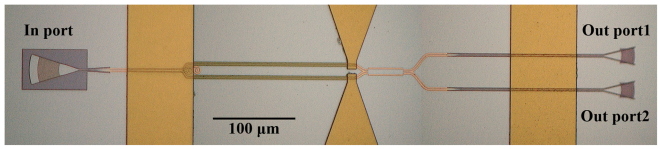

Fig. 5. The optical micrograph of the proposed device.

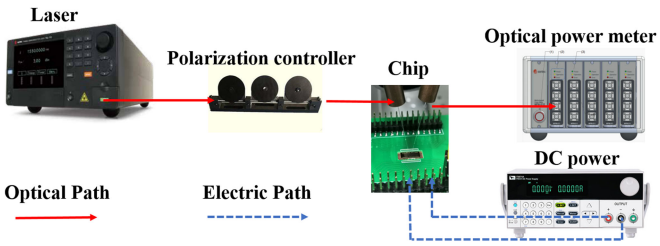

Fig. 6. Experiment setup for measurement.

TABLE I
Comparison of the Demonstrated Multi-Functional Devices with Polarizer and Power Splitter

Structure	Exp. or Sim.	Tunable	ER/IL @BW	Multiple etching
[13]	Sim.	No	>20 dB/<0.8 dB @180 nm	No
[14]	Sim.	No	>15 dB/<0.4 dB @118 nm	Yes
[18]	Exp.	No	>25 dB/<1 dB @100 nm	No
This work	Exp.	Beam-splitting ratio: 1:99 to 99:1	>14.9 dB/<1.73 dB @100 nm (S) Non/~3.71 dB @60 nm (E)	No

(S): Simulation result. (E): Experiment result. IL = Insertion Loss. ER = Extinction Ratio. Exp. = Experiment. Sim. = Simulation.

device is shown in Fig. 5. The schematic diagram of the measurement setup is shown in Fig. 6. The linearly polarized light is generated from the laser (TSL-710, Santec). By controlling the polarization controller, the TM polarized light will be input to a TM grating (In port) on the chip. After passing through the device, the input TM polarized light is converted into TE polarized light and output from the TE grating (Out port1 and Out port2). Then, the output TE polarized light is detected by an optical power meter (MPM-210, Santec). On the other hand, when we adjust the polarization controller to make the TE polarized light incident on the In port (TM grating), the TE polarized light cannot be efficiently input into the proposed device due to the huge coupling mismatch. At this time, the optical energy output at Out port1 and Out port2 is lower than the detection ranges of our optical power meter. Therefore, the measurement results of transmission characteristics in TE polarization are not given in this paper. For the same reason, the measurement result of polarization extinction ratio in Table I is empty (non).

Firstly, we measured the transmission spectrum of the proposed device, as shown in Fig. 7(a). It can be seen that the optical energy is mainly output from Out port1 and the minimum

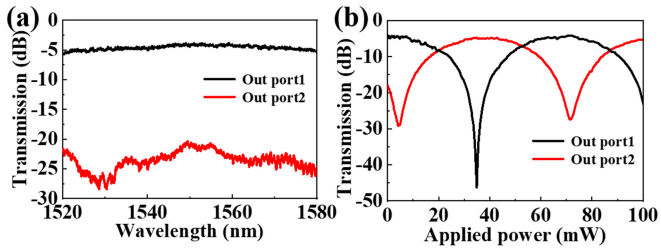

Fig. 7. (a) Measured transmittance spectra for the fabricated device. (b) Tunable beam- splitting ratio varies with applied power.

IL of the device is 3.71 dB at the wavelength of 1552.86 nm. The insertion loss mainly originates from the following parts: ∼0.22 dB caused by the adiabatic taper, ∼1.49 dB from the spatial mode order convertor, ∼0.36 dB from the MMI. In addition, the fabrication error between the fabricated device and simulated architecture is also a main reason for the insertion loss of the device. In the wavelength range of 1520–1580 nm, the ripple of insertion loss of the device is less than ± 0.97 dB, which is mainly caused by the jitter of MMI and adiabatic taper over a wide-band range.

To tune the beam-splitting ratio of two Out ports, we set a laser output wavelength to be 1550 nm and apply a voltage to the heater using a DC power. It can be seen from Fig. 7(b) that the beam-splitting ratio of the two Out ports is continuous tunable due to the continuous change of the applied power. The beam-splitting ratio of two Out ports can be adjusted from 1:99 to 99:1 within 33.2 mW power consumption. Such a beam-splitting ratio with a large adjustment range can meet the requirements of almost all beam splitters at present.

Finally, the performances of some reported multi-functional devices and our proposed device are summarized in Table I. It can be seen that our proposed device exhibits similar performance to the reported devices in terms of achieving multi-function. It is worthy to be noted that the proposed device is a novel multi-functional device with a polarizer and a power splitter that can realize reconfigurable beam-splitting ratio. Our device will greatly expand the applications of such a multi-functional device. In addition, the waveguide of our proposed device can be realized by one-step shallow etching, which is consistent with the processing technology of most SOI based devices and convenient for large-scale integration.

IV. Conclusion

In summary, we simulate and experimentally verify a TM-mode-pass polarization rotator and power divider based on SOI rib waveguide. The simulation results show that an ultrabroad operation bandwidth from 1500–1600 nm can be achieved when polarization extinction ratio (PER) is >14.9 dB for the TE_0 mode and the insertion loss (IL) is <1.73 dB for the TM_0 mode. Further, the proposed device is fabricated and measured. The measurement results show that when the TM_0 mode is launched from the In port, it will output from the Out port1 and Out port2 by the TM_0-TE_3-TE_0 mode conversion. When a voltage is applied to the heater, the steady-state power divider can be reconfigured from 1:99 to 99:1 within 33.2 mW of electrical power consumption. Therefore, both polarization selection-rotation and arbitrary power splitting in a single device are realized. Moreover, the device achieves a reconfigurable beam-splitting ratio, which makes the device highly competitive in a variety of multi-functional devices. Furthermore, with the features of compact footprint and thermal reconfiguration, the proposed device will have promising applications in large-scale integrated photonic circuits.

References

[1] V. Stojanovic et al., "Monolithic silicon-photonic platforms in state-of-the-art CMOS SOI processes," *Opt. Exp.*, vol. 26, no. 10, pp. 13106–13121, May 2018.
[2] H. Xu, D. Dai, and Y. Shi, "Ultra-broadband and ultra-compact on-chip silicon polarization beam splitter by using hetero-anisotropic metamaterials," *Laser Photon. Rev.*, vol. 13, no. 4, Apr. 2019, Art. no. 1800349.
[3] C. Li, M. Zhang, J. E. Bowers, and D. Dai, "Ultra-broadband polarization beam splitter with silicon subwavelength-grating waveguides," *Opt. Lett.*, vol. 45, no. 8, pp. 2259–2262, Apr. 2020.
[4] D. X. Dai and H. Wu, "Realization of a compact polarization splitter-rotator on silicon," *Opt. Lett.*, vol. 41, no. 10, pp. 2346–2349, May 2016.
[5] S. Wu, J. Hao, Z. Zhao, and X. S. Yao, "Low loss and high extinction ratio all-silicon TM-pass polarizer with reflection removal enabled by contra-mode conversion Bragg-gratings," *Opt. Exp.*, vol. 29, no. 17, pp. 27640–27652, Aug. 2021.
[6] M. Xu et al., "High-performance coherent optical modulators based on thin-film lithium niobate platform," *Nature Commun.*, vol. 11, no. 1, Aug. 2020, Art. no. 3911.
[7] K. Suzuki et al., "Low-loss, low-crosstalk, and large-scale optical switch based on silicon photonics," *J. Lightw. Technol.*, vol. 38, no. 2, pp. 233–239, Jan. 2020.
[8] D. Dai et al., "10-Channel mode (de)multiplexer with dual polarizations," *Laser Photon. Rev.*, vol. 12, no. 1, Jan. 2018, Art. no. 1700109.
[9] M. Khorasaninejad and K. B. Crozier, "Silicon nanofin grating as a miniature chirality-distinguishing beam-splitter," *Nature Commun.*, vol. 5, Nov. 2014, Art. no. 5386.
[10] S. M. Saimon et al., "A high sensitivity refractive index sensor based on leaky mode coupler of MMI," *IEEE Photon. Technol. Lett.*, vol. 34, no. 1, pp. 63–66, Jan. 2022.
[11] L. Han, B. P. P. Ku, N. Alic, and S. Radic, "Ultra-broadband multimode 3dB optical power splitter using an adiabatic coupler and a Y-branch," *Opt. Exp.*, vol. 26, no. 11, pp. 14800–14809, May 2018.
[12] M. H. Tahersima et al., "Deep neural network inverse design of integrated photonic power splitters," *Sci. Rep.*, vol. 9, Feb. 2019, Art. no. 1368.
[13] B. Ni and J. Xiao, "Ultracompact and broadband silicon-based TE-pass 1x2 power splitter using subwavelength grating couplers and hybrid plasmonic gratings," *Opt. Exp.*, vol. 26, no. 26, pp. 33942–33955, Dec. 2018.
[14] Z. Guo and J. Xiao, "Silicon-based ultracompact TE-pass/TM-stop power divider using subwavelength gratings assisted with segmented hybrid plasmonic horizontal slot waveguides," *J. Lightw. Technol.*, vol. 35, no. 19, pp. 4329–4336, Oct. 2017.
[15] M. Lu et al., "Ultra-compact TE-mode-pass power splitter based on subwavelength gratings and hybrid plasmonic waveguides on SOI platform," *Opt. Commun.*, vol. 498, Nov. 2021, Art. no. 127250.
[16] M. Lin et al., "Star-type polarizer with equal-power splitting function for each polarization based on polarization-dependent defects in two-dimensional photonic-crystal waveguides," *Opt. Exp.*, vol. 24, no. 21, pp. 23917–23924, Oct. 2016.
[17] C. Deng et al., "Reconfigurable and low-power consumption polarization rotating beam splitter with EIT-like effect based on SOI ridge waveguide," *Opt. Commun.*, vol. 495, Sep. 2021, Art. no. 127054.
[18] H. Zafar, R. Flores, R. Janeiro, A. Khilo, M. S. Dahlem, and J. Viegas, "High-extinction ratio polarization splitter based on an asymmetric directional coupler and on-chip polarizers on a silicon photonics platform," *Opt. Exp.*, vol. 28, no. 15, pp. 22899–22907, Jul. 2020.